Biochimica et Biophysica Acta 1850 (2015) 1140–1149

Contents lists available at ScienceDirect

Biochimica et Biophysica Acta

journal homepage: www.elsevier.com/locate/bbagen

Tat PTD–endostatin: A novel anti-angiogenesis protein with ocular barrier permeability *via* eye-drops

Xinke Zhang [a], Yan Li [b], Yanna Cheng [a], Haining Tan [c], Zhiwei Li [d], Yi Qu [e], Guoying Mu [d], Fengshan Wang [b,*]

[a] Department of Pharmacology, School of Pharmaceutical Sciences, Shandong University, Jinan, China
[b] Key Laboratory of Chemical Biology of Natural Products (Ministry of Education), Institute of Biochemical and Biotechnological Drugs, School of Pharmaceutical Sciences, Shandong University, Jinan, China
[c] National Glycoengineering Research Center, Shandong University, Jinan, China
[d] Department of Ophthalmology, Provincial Hospital Affiliated to Shandong University, Jinan, China
[e] Department of Health Care, QiLu Hospital of Shandong University, Jinan, China

ARTICLE INFO

Article history:
Received 29 August 2014
Received in revised form 28 December 2014
Accepted 30 January 2015
Available online 4 February 2015

Keywords:
Tat PTD
Endostatin
Fusion protein
Ocular barrier
CNV

ABSTRACT

Background: Endostatin, a specific inhibitor of endothelial cell proliferation and angiogenesis, has been proved to have effects on ocular neovascular diseases by intraocular injection. In order to increase its permeability to ocular barriers and make it effective on fundus oculi angiogenesis diseases *via* non-invasive administration (eye drops), endostatin was fused to Tat PTD *via* a genetic engineering method.
Methods: Most of the Tat PTD– endostatin was expressed as inclusion bodies in *Escherichia coli*, so pure and active Tat PTD–endostatin was prepared by a series of operations, including inclusion body denaturation, refolding and chromatography. The anti-angiogenesis activity of Tat PTD–endostatin was investigated by cell proliferation experiments and chick embryo chorioallantoic membrane assay. In addition, its translocating ability and concrete entry mechanism into cells were also investigated by fluorescence microscope and flow cytometry. The penetrating ability to ocular barriers was also studied by immunohistochemistry. A mouse choroidal neovascularization model was established to investigate the pharmacodynamics of Tat PTD–endostatin.
Results: The obtained Tat PTD–endostatin had excellent anti-angiogenesis activity and was superior to Es in cellular translocating. Macropinocytosis may be the dominant route of entry of Tat PTD–endostatin into cells. Tat PTD–endostatin could cross ocular barriers and arrive at the retina after eye-drop administration. In addition, it displayed inhibitory effects on choroidal neovascularization *via* eye drops.
Conclusions: Tat PTD–endostatin possessed excellent ocular penetrating ability and anti-angiogenesis effects.
General significance: Tat PTD is a promising ocular delivery tool, and Tat PTD–endostatin is a potential drug for curing fundus oculi angiogenesis diseases.

1. Introduction

Endostatin (Es), a 20 kDa *C*-terminal fragment of collagen XVIII, is a specific inhibitor of endothelial cell proliferation and angiogenesis [1–4]. Its analogue, Endostar, has been approved by the China Food and Drug Administration (CFDA) for the treatment of patients with non-small-cell lung cancer [5]. In addition, researchers have made some achievements with Es on the prevention and treatment of ocular neovascular diseases [6]. For example, researchers have identified that Es and the Es gene could inhibit ocular neovascularization by bulbar conjunctival injection or intravitreal injection [7,8]. However, due to ocular barriers, Es has to be administered by intraocular injection to cure fundus oculi diseases. This mode of operation is difficult and can result in irreversible damage to the eyeball [9], and so it is critical to develop a simple, safe and effective route for the administration of Es to treat these ocular diseases. Although eye-drops seem to be an ideal administration route, ocular barriers prevent penetration of Es into fundus oculi sites.

Tat PTD, a protein transduction domain of the Tat protein of HIV-1, has been studied extensively for its ability to pass through biological membranes with different cargoes, including peptides, proteins, and oligonucleotides [10–13]. Many *in vitro* and *in vivo* studies have shown that Tat PTD and its cargos [14,15] were able to pass through most cell line membranes [16]. After being fused with Tat PTD, some proteins with poor cell membrane permeability could cross the blood–brain barrier (BBB) and even the eye barriers [12,17–19]. It is,

Abbreviations: Es, endostatin; Tat PTD, protein transduction domain of Tat; Tat PTD–Es, Tat PTD–endostatin; CAM, chorioallantoic membrane; BBB, blood–brain barrier; EDTA, ethylene diamine tetraacetic acid; bFGF, basic fibroblast growth factor; NS, normal saline; CNV, choroidal neovascularization

* Corresponding author.
E-mail address: fswang@sdu.edu.cn (F. Wang).

http://dx.doi.org/10.1016/j.bbagen.2015.01.019
0304-4165/

therefore, a promising tool for non-invasive cellular import of cargos and for making therapeutic agents more efficient for the treatment of many diseases. We hypothesized that Tat PTD might assist Es in penetrating the ocular barriers and playing its anti-angiogenesis role on the fundus oculi *via* eye-drops.

Thus, in this study, Tat PTD was conjugated to the *N*-terminus of Es through a bioengineering method and expressed in *Escherichia coli*. After a series of operations, including inclusion body denaturation, refolding and chromatography, pure Tat PTD–Es, which was expected to have both ocular barrier-penetrating ability and anti-angiogenesis effects, was obtained. In order to verify whether the purified Tat PTD–Es possesses ocular penetrating ability and anti-angiogenesis effects, its *in vitro* and *in vivo* activities were investigated. The anti-angiogenesis activity of Tat PTD–Es *in vitro* was determined using cell proliferation experiments and the chorioallantoic membrane (CAM) assay. The ocular barrier-penetrating activity and inhibitory activity on choroidal neovascularization (CNV) of Tat PTD–Es *via* eye-drops were evaluated *in vivo*. Furthermore, its concrete entry mechanism into cells was also investigated, since understanding its mechanism will aid in its application in clinical treatment.

2. Materials and methods

2.1. Strains, vectors, cells and reagents

E. coli DH5α cells were used for plasmid propagation and *E. coli* BL21 (DE3) cells were used for expression of the fusion protein. A His-trap™ HP column, was purchased from GE Healthcare (Sweden). EAHY926 endothelial cells were obtained from Shanghai Cell Bank, the Institute of Cell Biology, China Academy of Sciences (Shanghai, China). Avastin was produced by Genentech/Roche (US). Mouse anti-His polyclonal antibody was purchased from Zhongshan Golden Bridge Biotechnology Co. Ltd (Beijing, China). Fertilized eggs were purchased from Yijia Chicken Farm (Jinan, China). Cell Counting Kit-8 (CCK-8) was purchased from Shanghai Beibo Company (China). LPS ELISA Kit was purchased from Wuhan ColorfulGene Company (China). All other reagents of biochemical and molecular biology grade were obtained from Sigma-Aldrich (China).

2.2. Animals

Kunming mice, weighing 25–28 g, were purchased from the Experimental Animal Center of Shandong University. Five-week-old male C57BL/6 mice, weighing 20–22 g, were purchased from Beijing Vital River Company. The animals were housed in animal facilities accredited by the Shandong Council on Animal Care and treated in accordance with approved protocols. The animals were maintained in a specific pathogen-free environment that was temperature-controlled (23 °C ± 2 °C) and humidity-controlled (60% ± 10%), under a 12:12-h light/dark cycle.

2.3. Construction of a recombinant plasmid expressing Tat PTD–Es in E. coli

Tat PTD–Es cDNA was amplified from the plasmid pVAX1-endostatin by a standard polymerase chain reaction (PCR) with the forward primer F1 (5′-AGAATCCCATATGTATGGCAGGAAGAAGCGGAGACAGCGACGAA GACACAGCCACCGCGA-3′) and reverse primer R (5′-CGCGG ATCCTTAT TACTTGGAGGCAGTCATGAA-3′). The forward primer F1 and reverse primer R contained *Nde* I and *Bam* HI sites, respectively. A 562-bp amplified fragment was cut with *Nde* I and *Bam* HI and then ligated into the pET28a vector that had been previously digested with *Nde* I and *Bam* HI, to create the corresponding expression vector pET28a/Tat PTD–Es. Another expression vector, pET28a/Es, was generated *via* the same procedure as above using the forward primer F2 (5′-AGGAATCCCATATGCA CAGCCACCGCGACTT-3′) and reverse primer R. The accuracy of the inserted genes was confirmed by DNA sequencing.

2.4. Expression, renaturation and purification of the proteins

E. coli BL21 (DE3) cells containing the recombinant plasmid were cultured at 37 °C in LB medium containing 50 μg ml^{-1} kanamycin with a shaking speed of 220 rpm. When the OD600 of the culture reached 0.8–1.0, isopropyl-β-D-thiogalactopyranoside (IPTG) was added to a final concentration of 0.25 mM. After a further 6-h cultivation, the cells were harvested and subjected to sonication. After centrifugation at 10,000 ×*g* for 30 min, the obtained inclusion bodies were washed with Tris–HCl buffer (20 mM Tris–HCl, 0.5% Triton X-100, pH 8.2) and Tris–HCl–urea buffer (20 mM Tris–HCl, 0.5% Triton X-100, 1 M urea, pH 8.2). The precipitate was then dissolved in denaturing buffer (20 mM Tris–HCl, 8 M urea, 5 mM ethylene diamine tetraacetic acid (EDTA), pH 8.2, 10 mM dithiothreitol). The denaturing liquid was subjected to slow dilution into the refolding buffer (20 mM Tris–HCl buffer, 2 M urea, 0.25 M oxidized glutathione, 0.1 mM reduced glutathione, pH 8.2) in a volume ratio of 1:100 at 4 °C. The solution was left standing for 24 h, ultrafiltrated to one-tenth of the total volume through a ultrafiltration membrane with a molecular weight cut-off of 10 kDa, and then washed with Tris–HCl buffer (20 mM, pH 8.0) containing 0.3 M NaCl. Subsequently, the protein solution was loaded onto a His-trap™ HP column and the fusion proteins were eluted with Tris–HCl buffer (20 mM, pH 8.0) containing 0.3 M NaCl and 100 mM imidazole. The fractions containing fusion proteins were then ultrafiltrated to remove NaCl and imidazole. Throughout the whole process, the fusion protein fractions were analysed by SDS-PAGE. The immunoreactivity of fusion protein was checked by Western blotting. Mouse anti-His-tag monoclonal antibody was used as the primary antibody.

The concentration of lipopolysaccharides (LPS) in samples was determined by LPS ELISA Kit. Tat PTD–Es and Es were diluted to 10 μM, 50 μM and 100 μM with normal saline. The assay of LPS in the samples was strictly operated by LPS ELISA Kit protocol.

2.5. Endothelial cell proliferation assay

EAHY926 endothelial cells were washed with PBS and digested in 0.05% trypsin solution. A cell suspension of 30,000 cells/ml was made with DMEM plus 10% FBS, plated onto gelatinized 96-well culture plates (0.1 ml/well), and incubated (37 °C, 5% CO_2) for 12 h. Tat PTD–Es and Es were diluted with the culture media. After 20 min of incubation, the culture media and basic fibroblast growth factor (bFGF) were added to obtain a final volume of 0.2 ml of DMEM + 10% FBS + 5 ng ml^{-1} bFGF. Cellular viability was assessed using CCK-8 according to the manufacturer's instructions.

2.6. Chick embryo CAM assay

Inhibition of angiogenesis by Tat PTD–Es and Es *in vivo* was tested in a chick embryo CAM assay with some changes to the previously described method [20,21]. Briefly, 3-day-old fertilized white leghorn eggs were incubated at 37 °C and 40–60% humidity for 3 days, with rotation every day. An artificial window (1–2 cm) was gently cut on day 4. On day 7, a small piece of gelatin sponge (0.5 cm length, 0.5 cm width) saturated with different solutions was placed on the areas between pre-existing vessels. For the three control groups, the gelatin sponge was treated with 60 μg hydrocortisone, sterile saline or 0.5 ng bFGF, respectively. Additionally, for the two test groups, 0.5 nM Tat PTD–Es or Es and 0.5 ng bFGF were added onto the gelatin sponge. The embryos were further incubated for 48 h. The zones of neovascularization under and around the gelatin sponge were photographed using an anatomic microscope (Leica, MS5, Switzerland). Quantitative analyses were performed with the Image-pro plus 6.0 image analysis software.

2.7. In vitro cellular uptake of Tat PTD–Es and Es

To examine whether the transduction efficiency into EAHY926 cells could be enhanced, cellular uptake studies were performed. The abilities of cellular internalization of Tat PTD–Es and Es were visualized and quantified using a fluorescence microscope (BX40, Olympus, Japan) and flow cytometry, respectively. To track the internalization of proteins, Tat PTD–Es and Es labelled with FITC were prepared as previously described [22]. EAHY926 cells were seeded in 12-well culture plates at 1.0×10^5 cells/well. The culture medium was removed after the cells reached 80% confluence and the cells were treated with fresh serum-free medium containing 10 μM FITC-labelled Tat PTD–Es and Es for 4 h at 37 °C with 5% CO_2 in an incubator. Sequentially, the cells were examined under a fluorescence microscope and the fluorescence signal was determined by flow cytometer.

2.8. Studies on the cellular uptake pathway of Tat PTD–Es

To further understand the concrete uptake mechanism of Tat PTD–Es by cells, the impact of concentration, time, temperature and some inhibitors on the transduction of Tat PTD–Es was studied using a fluorescence microscope (BX40, Olympus, Japan) and flow cytometry respectively. To examine the effects of Tat PTD–Es concentration and action time on transduction efficiency, the cells were incubated with the FITC-labelled Tat PTD–Es or Es at different concentrations (1, 2.5, 5, 7.5 and 10 μM) for various time periods from 15 min to 4 h. The effect of temperature block was studied by pre-incubating the cells at 4 °C for 1 h and then treating with the FITC-labelled Tat PTD–Es (10 μM) for 2 h at 4 °C. To study the effect of various inhibitors on the uptake of Tat PTD–Es, cells were pre-incubated with the following inhibitors individually at concentrations that were not toxic to the cells: (1) 0.1% (w/v) sodium azide for 1 h; (2) 450 mM sucrose for 1 h; (3) 10 μg ml^{-1} chlorpromazine for 30 min; (4) 1 μg ml^{-1} genistein for 30 min; (5) 30 mM cytochalasin D for 30 min. Following the pre-incubation, the cells were further treated with FITC-labelled Tat PTD–Es (10 μM) for 2 h. Subsequently, the cells were washed three times with PBS, collected according to the methods described above, and analysed by flow cytometry and fluorescence microscope, respectively. In the study, the group without any treatment was used as a background in the flow cytometry analysis, while the group in the presence of Tat PTD–Es, but without inhibitor treatment, was used as the control, and their fluorescence intensities are expressed as 100%. Comparing the fluorescence intensities of other groups with the intensity of the control group could extrapolate the possible mechanism of internalization.

2.9. Penetration of Tat PTD–Es through ocular barriers

Twenty-five Kunming mice were randomly divided into five groups: (1) normal saline (NS) negative control group — mice were administered 10 μl NS solution *via* eye-drops for 3 days (6 times per day); (2) Es eye-drops group — mice were administered 10 μl Es solution (50 μM) for 3 days (6 times per day); (3) Tat PTD–Es eye-drops group — mice were administered 10 μl Tat PTD–Es solution (50 μM) for 3 days (6 times per day); (4) Es intravitreal injection group — mice were intravitreally injected with 1 μl Es solution (50 μM); (5) Tat PTD–Es intravitreal injection group — mice were intravitreally injected with 1 μl Tat PTD–ES solution (50 μM).

The solutions were administered to the left eyes of the mice, while the right eye had no treatment. The mice of the eye-drop groups (groups 1, 2, 3) were executed after the last administration. The left eyeballs were removed and then cleaned using PBS. Eyeballs were fixed in 4% paraformaldehyde solution overnight. Cryosection was used to make slices of mouse eyeballs. Immunohistochemistry analysis using an anti-6 × His monoclonal antibody was used to observe whether the protein was distributed in the retina.

2.10. Inhibitory effects of Tat PTD–Es on CNV

A CNV model was generated by the modification of a previously described technique [6,23]. Briefly, 5-week-old male C57BL/6 mice were anaesthetized with chloral hydrate (4%, 0.14 ml/10 g), and the pupils were dilated with 1% tropicamide. Four burns of krypton laser photocoagulation (50 μm spot size, 0.1-second duration, 160 mW) were delivered to each retina using the slit-lamp delivery system and a hand-held cover slide as a contact lens. Production of a bubble during the laser treatment, which indicates rupture of the Bruch's membrane, is an important factor in obtaining CNV, so only the mice in which a bubble was produced for all four burns were included in the study. The left eyes were subjected to this treatment, while the right eyes had no treatment.

Thirty of the CNV model C57BL/6 mice were randomly divided into six groups: (1) normal saline (NS) negative control group — mice administered 10 μl NS solution *via* eye-drops for 2 weeks (6 times per day); (2) Avastin intravitreal injection positive group — mice were intravitreally injected with 1 μl Avastin for 2 weeks (once per week); (3) Tat PTD–Es eye-drops group — mice were administered 10 μl Tat PTD–Es solution (50 μM) for 2 weeks (6 times per day); (4) Tat PTD–Es intravitreal injection group — mice were intravitreally injected with 1 μl Tat PTD–ES solution (50 μM) for 2 weeks (once per week); (5) Es eye-drops group — mice were administered 10 μl ES solution (50 μM) for 2 weeks (6 times per day); (6) Es intravitreal injection group — mice were intravitreally injected with 1 μl Es solution (50 μM) for 2 weeks (once per week). The solution was administered to their left eyes, while the right eye had no treatment.

Fifteen days after treatment, the size of the CNV lesion was evaluated by measuring the area of CNV in choroidal flat mounts. The mice used for the flat-mount technique were anaesthetized and perfused with 1 ml PBS containing 50 mg ml^{-1} fluorescein-labelled dextran as previously described [8]. The eyeballs were removed and fixed for 1 h in 10% formalin solution. The cornea and lens were removed and the entire retina was carefully dissected from the eyeballs. Radial cuts were made from the edge of the eyecup to the equator and the eyecup was flat-mounted in aqua mount with the sclera facing down and the choroid facing up. The flat mounts were examined and the images were digitized.

3. Results

3.1. Cloning, expression, renaturation and purification of Tat PTD–Es and Es

In this study, the Tat PTD sequence (YGRKKRRQRRR) was fused to the *N*-terminus of Es protein and the fusion protein contained an *N*-terminal polyhistidine purification tag (His-tag). The recombinant fusion protein was expressed in *E. coli* at a level up to 20% of the total cell proteins, and most of the fusion protein was detected as inclusion bodies (Fig. 1). The molecular weight of Tat PTD–Es was 22 kDa, which was consistent with the size deduced from its coding sequence. The purity of the fusion protein was >95%, evaluated by SDS-PAGE (Fig. 2a). The final production of Tat PTD–Es was 20 mg ml^{-1} of cell culture. Western blot analysis showed that Tat PTD–Es and Es reacted with anti-6 × His antibody (Fig. 2b).

The concentration of LPS in samples was all lower than 10 pg ml^{-1} (the minimal assay range of LPS ELISA Kit) and there was no dose–concentration relationship, which proved that LPS was absent in samples and the production of recombinant proteins had reasonable quality. Test for absence of LPS assured that the preparation would not induce inflammatory reaction when used *in vivo*.

3.2. Inhibitory effect of Tat PTD–Es on endothelial cell proliferation

A CCK-8 assay was performed to investigate the anti-proliferative effects of Tat PTD–Es and Es (Fig. 3). Both of the two proteins significantly

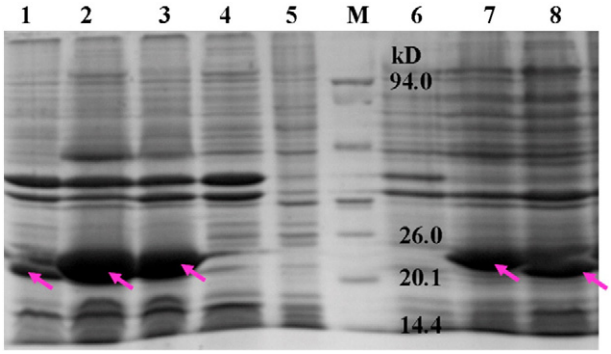

Fig. 1. SDS-PAGE of proteins from engineered strains. *Lane 1*. Inclusion bodies of BL21(DE3)/Es; *Lanes 2 and 3*. Inclusion bodies of BL21(DE3)/Tat PTD–Es; *Lane 4*. Inclusion bodies of BL21(DE3)/blank plasmid; *Lane 5*. The cell lysate of BL21(DE3); *M*. protein marker; *Lane 6*. The cell lysate of BL21(DE3)/blank plasmid; *Lane 7*. The cell lysate of BL21(DE3)/Tat PTD–Es; *Lane 8*. The cell lysate of BL21(DE3)/Es.

inhibited bFGF-induced EAHY926 endothelial cell proliferation in a dose-dependent manner. The inhibitory rates of Tat PTD–Es at 0.2, 0.8, 2, 3, 4 and 8 μM were 25.09%, 38.36%, 65.55%, 75.64%, 83.94% and 86.45%, respectively. For Es, the inhibitory rates were 10.35%, 28.24%, 59.67%, 70.34%, 82.38% and 88.04%, respectively. Addition of Tat PTD at the *N*-terminus of Es did not decrease the endothelial cell proliferation inhibitory activity. Both Tat PTD–Es and Es showed more than 80% inhibition of bFGF-induced EAHY926 endothelial cell proliferation at high concentrations (4 and 8 μM). Tat PTD–Es even displayed an enhanced inhibitory effect compared with Es ($p < 0.05$) at low concentrations (0.2 and 0.8 μM).

3.3. Inhibitory effect of Tat PTD–Es on angiogenesis in the chick embryo CAM

To further study the anti-angiogenesis activity, Tat PTD–Es and Es were tested using a CAM assay. Tat PTD–Es and Es inhibited the development of new embryonic blood vessels without affecting pre-existing vasculature (Fig. 4), suggesting that Tat PTD–Es and Es could significantly inhibit angiogenesis of CAM induced by bFGF. Compared with the bFGF group, the number of blood vessels of CAM was reduced from 30.74 ± 6.58 to 12.18 ± 4.92 in the Tat PTD–Es group (Fig. 4).

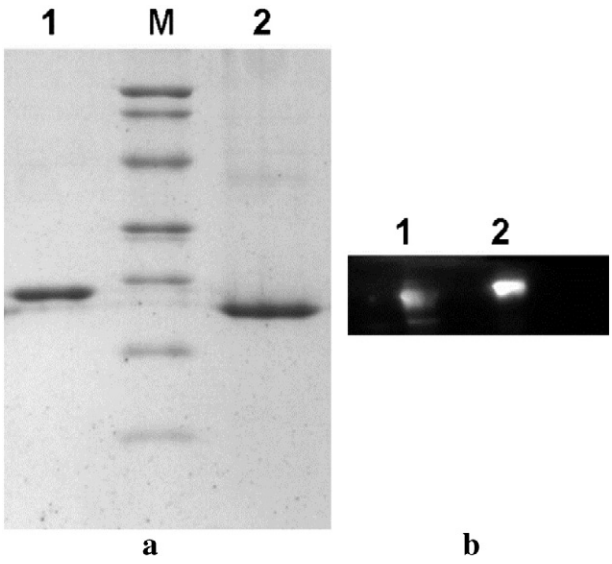

Fig. 2. SDS-PAGE and Western blotting of the purified Tat PTD–Es and Es. a. SDS-PAGE of purified Tat PTD–Es and Es. *Lane 1*. Purified Tat PTD–Es; *Lane 2*. Molecular marker; *Lane 3*. Purified Es. b. Western blotting of purified proteins. *Lane 1*. Es; *Lane 2*. Tat PTD–Es.

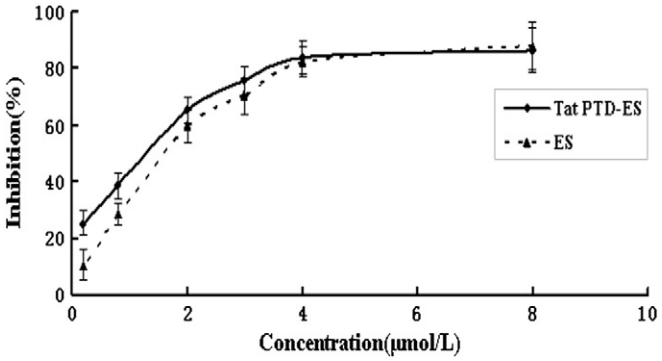

Fig. 3. The inhibitory effect of Tat PTD–Es and Es on EAHY926 cell proliferation.

3.4. In vitro cellular uptake of Tat PTD–Es

Fluorescent micrographs of cells taken at 4 h after exposure to Tat PTD–Es and Es are shown in Fig. 5a. Intracellular accumulation of FITC-labelled protein was observed, and the fluorescence intensity in cells exposed to Tat PTD–Es increased notably compared with Es. The percentage of cells that internalized the FITC-labelled proteins was quantified by flow cytometry (Fig. 5b and c). The percentage of positive cells after exposure to Tat PTD–Es and Es was 99.28% and 33.61%, respectively. The results indicate that Tat PTD significantly enhanced Es delivery into EAHY926 cells ($p < 0.05$).

3.5. Cellular uptake pathway of Tat PTD–Es

The uptake of Tat PTD–Es by EAHY926 cells was clearly dependent on the tested concentration range of 1–10 μM (Fig. 6a). When the concentration increased, the fluorescence intensity in EAHY926 cells increased accordingly (Fig. 6b). In terms of the effect of the treatment time on the internalization process of Tat PTD–Es, the fluorescence intensity inside EAHY926 cells increased with incubation time (Fig. 7a). Rapid entrance of Tat PTD–Es into cells was observed, and the fluorescence intensity increased sharply from 0 min to 2 h (Fig. 7b).

Endocytic uptake is an energy-dependent mechanism that can be strongly inhibited by lowering the temperature and by metabolic inhibitors [24]. In order to investigate whether the cellular uptake of Tat PTD–Es was an energy-dependent process, the cell uptake studies were carried out at 4 °C and also in the presence of metabolic inhibitors (sodium azide, NaN_3) [25]. The group in the presence of Tat PTD–Es at 37 °C, but without inhibitor treatment, was used as a control, and its fluorescence intensities are expressed as 100% (Fig. 8). It can be seen from Fig. 8a that the uptake of Tat PTD–Es in EAHY926 cells was inhibited but not abolished completely at low temperature or in the presence of NaN_3 in comparison with the control group. Low temperature decreased the accumulation of Tat PTD–Es in EAHY926 cells by more than 90%. Similarly, the cellular metabolism was also significantly inhibited by NaN_3 with a cellular uptake reduction of 94%. The results of the low temperature and metabolic inhibitor assays indicate that Tat PTD–Es is taken up into the cells *via* an energy-dependent process. However, Tat PTD–Es might be taken up by different pathways, resulting in the differences in their degrees of inhibition. Therefore, endocytic inhibitors were used to investigate the uptake pathway of Tat PTD–Es in EAHY926 cells.

Exposure of cells to hypertonic media, such as sucrose, is known to inhibit fluid-phase endocytosis [26]. When treated with sucrose (450 mM) for 1 h, the uptake of Tat PTD–Es into EAHY926 cells was reduced by 63% ($p < 0.01$, Fig. 8b). Hypertonic sucrose is known to block the formation of the clathrin-coated vesicles and the results suggest that Tat PTD–Es entered EAHY926 cell by clathrin-mediated endocytosis. Inhibition of clathrin-mediated uptake was also tested by using the cationic amphiphilic drug chlorpromazine, which is believed to

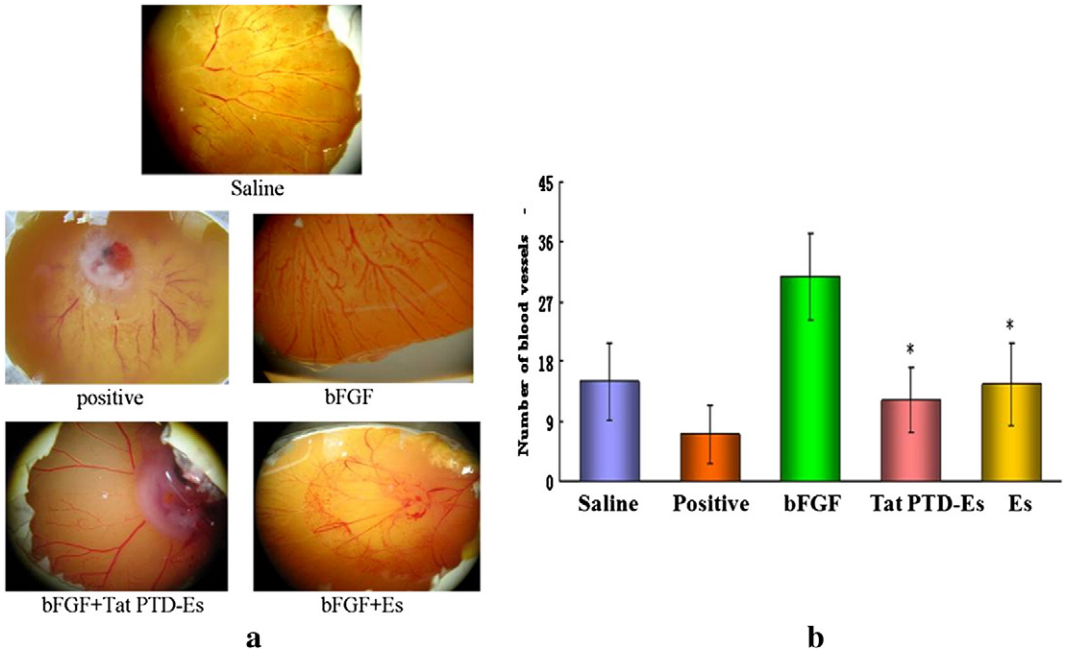

Fig. 4. Inhibitory effects of Tat PTD–Es and Es on chick embryo CAM. a. Photographs of angiogenesis of CAM. b. The inhibitory activity on CAM angiogenesis (*$p < 0.05$ compared to the bFGF group).

inhibit clathrin-coated pit formation by a reversible translocation of clathrin and its adapter proteins from the plasma membrane to intracellular vesicles and causes clathrin to accumulate in late endosomes, thereby inhibiting coated pit endocytosis [27]. Treatment with chlorpromazine (10 μg ml^{-1}) for 30 min resulted in obvious inhibition of Tat PTD–Es uptake into EAHY926 cells, which also indicates that

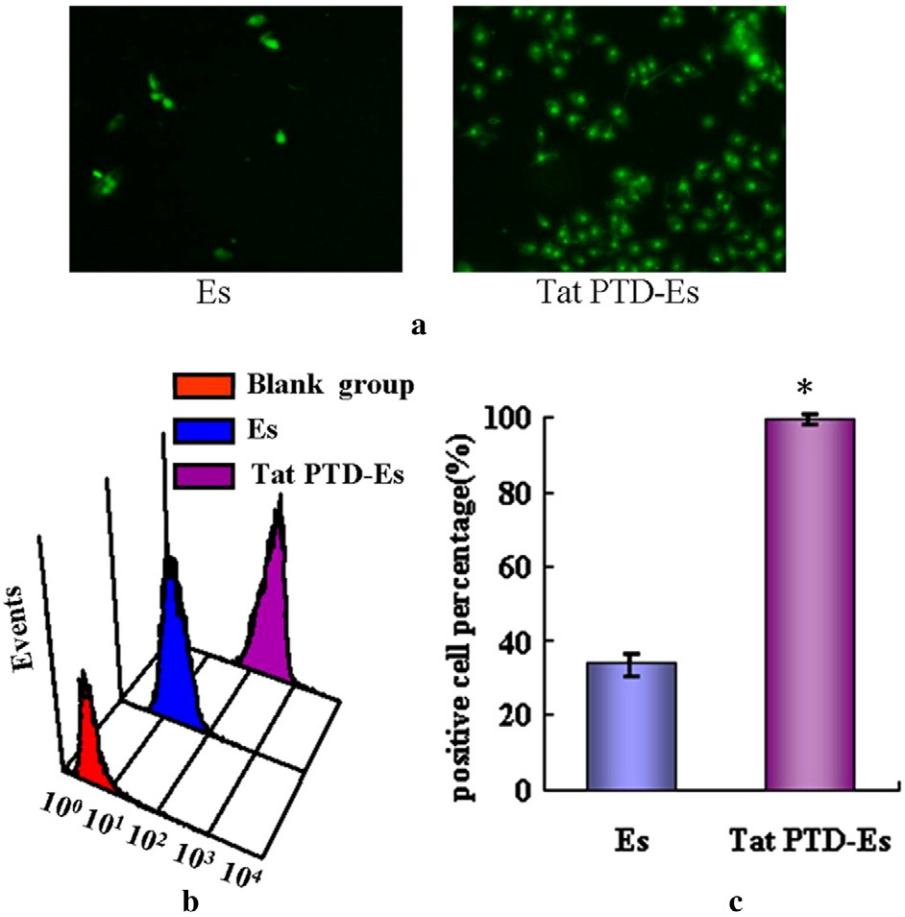

Fig. 5. Transduction of Tat PTD–Es and Es into EAHY926 cells. a. Fluorescent microscopy image of FITC-labelled Tat PTD–Es and Es incubated with EAHY926 cells (×200). b. Flow cytometry profiles of EAHY926 cells after exposure to FITC-labelled Tat PTD–Es and Es. c. The positive rates of cells exposed to Tat PTD–Es and Es.

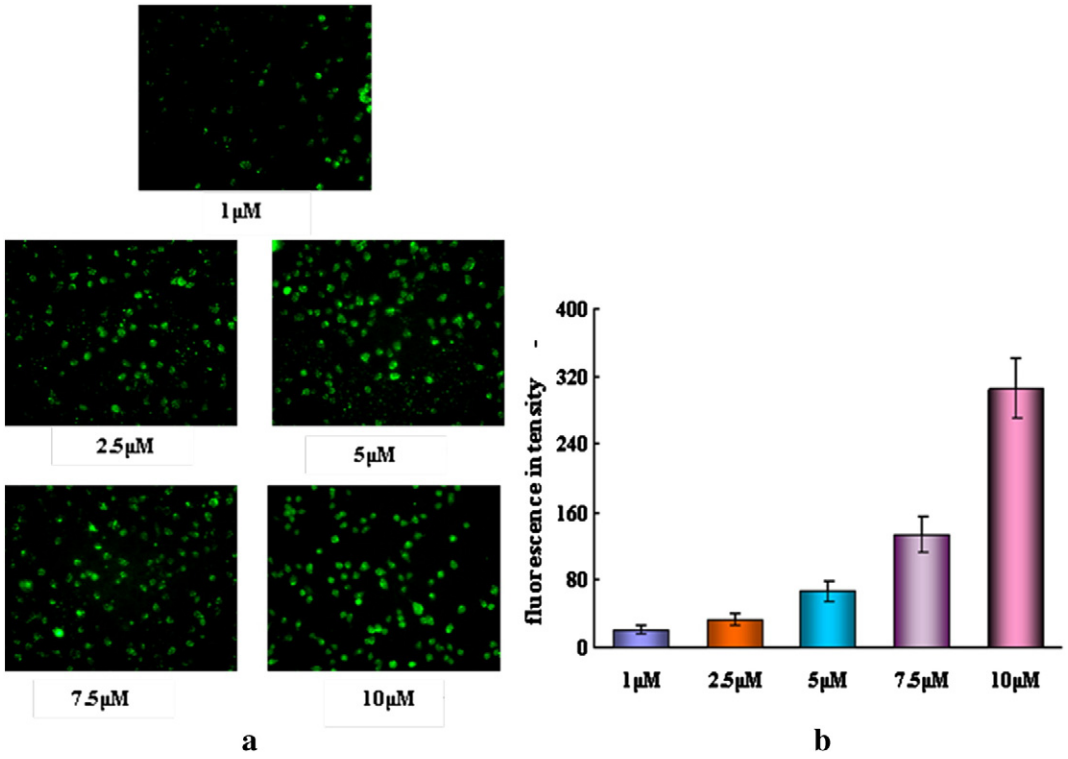

Fig. 6. The effect of concentrations on uptake of Tat PTD–Es and Es into EAHY926 cells. a. Fluorescent microscope images of EAHY926 cells incubated with different concentrations of FITC-labelled Tat PTD–Es and Es (×200). b. Uptake of Tat PTD–Es by EAHY926 cells at different concentrations of Tat PTD–Es.

clathrin-mediated endocytosis might be involved in the uptake process in EAHY926 cells.

Genistein, a tyrosine kinase inhibitor that causes local disruption of the actin network at the site of endocytosis and inhibits the recruitment of dynamin II, has been shown to inhibit the caveolae-mediated endocytosis of SV40 virus and cholera toxin X [28]. In this study, when cells were pre-incubated with genistein (1 μg ml^{-1}) for 30 min, the cellular uptake of Tat PTD–Es was inhibited significantly by 33%, indicating that a portion of Tat PTD–Es was internalized into the cells through caveolae-mediated endocytosis.

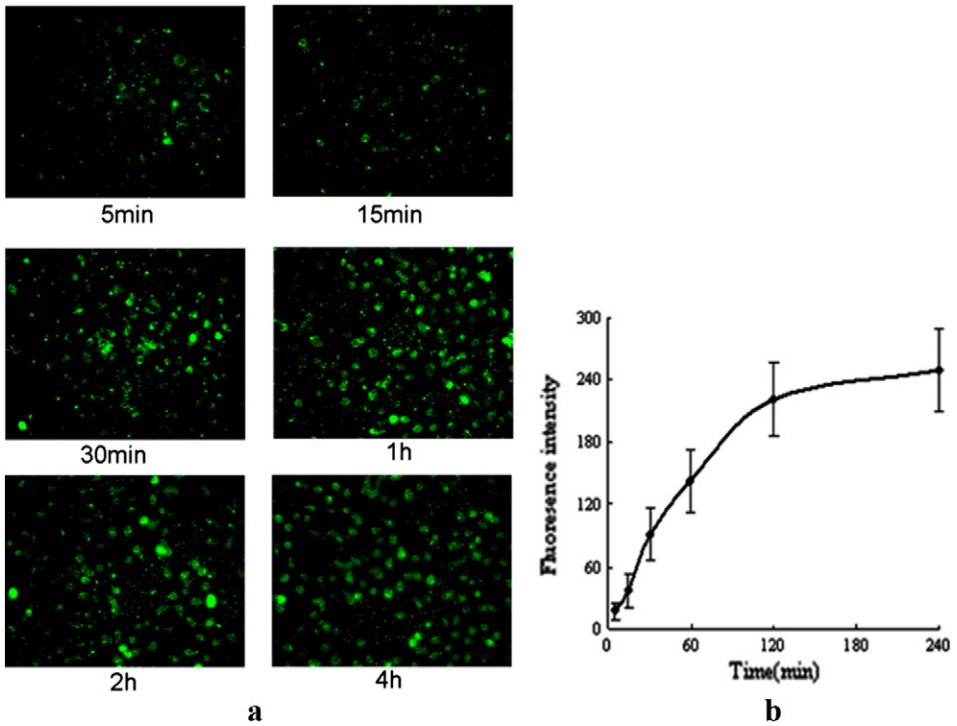

Fig. 7. Uptake of Tat PTD–Es by EAHY926 cells at different treatment times. a. Fluorescent microscopy images of EAHY926 cells at different treatment times (×200). b. The uptake of Tat PTD–Es by EAHY926 cells at different treatment times.

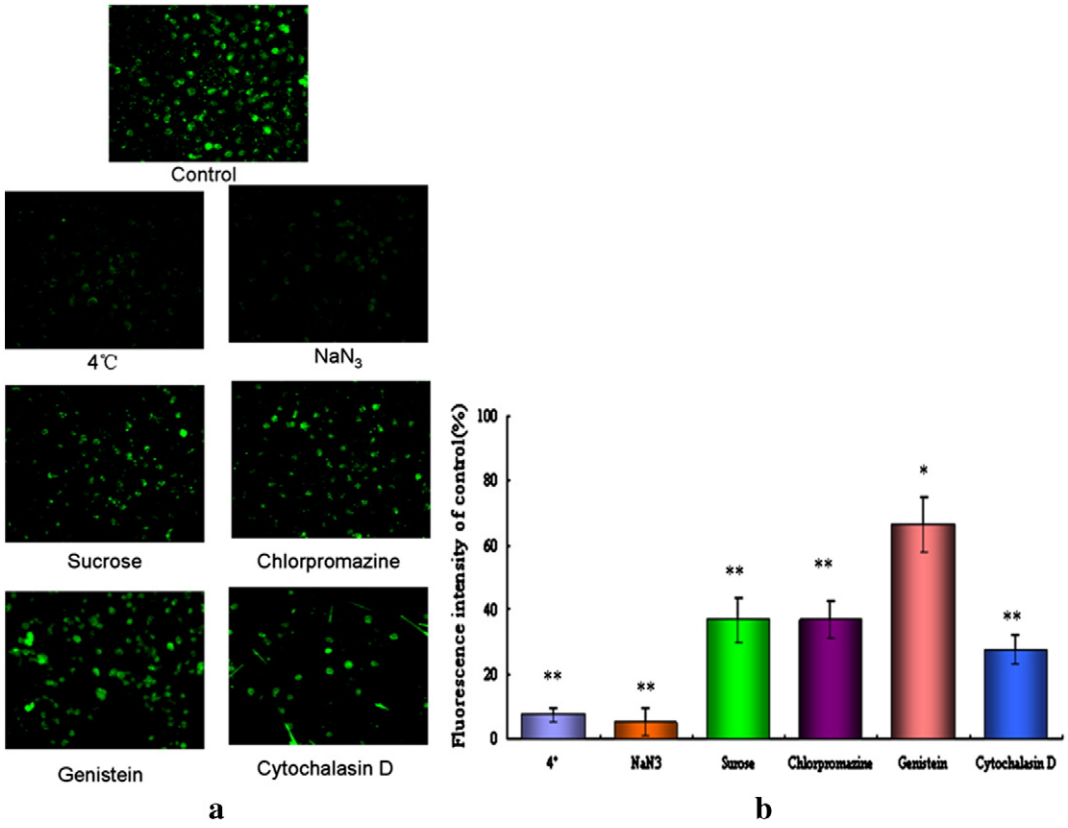

Fig. 8. Influence of different pathway inhibitors on the uptake of Tat PTD–Es by EAHY926 cells. a. Fluorescent microscopy images of EAHY926 cells with different treatments (×200). b. Uptake of Tat PTD–Es by EAHY926 cells with different treatments compared with control, $^{*}p < 0.05$, $^{**}p < 0.01$. The group in the presence of Tat PTD–Es without inhibitor treatment was used as a control and its fluorescence intensities are expressed as 100%. The fluorescence intensities of other groups are shown as relative fluorescence intensities compared with the control.

Cytochalasin D is known to inhibit actin polymerization and membrane ruffling, which is involved in macropinocytosis and phagocytosis [29]. The cellular uptake of Tat PTD–Es was significantly reduced by 72% after the cells were treated with cytochalasin D (30 mM) for 30 min. The results imply that macropinocytosis might be a major uptake mechanism for Tat PTD–Es by EAHY926 cells.

3.6. Ocular barrier penetrating ability of Tat PTD–Es

Tat PTD–Es or Es was eye-dropped or intravitreally injected. The NS group was employed as negative group. Mouse eyeballs were removed, and the fusion protein was examined with 6 × His antibody by immunohistochemistry (Fig. 9). Both Tat PTD–Es and Es appeared in the retina after intravitreal injection. Tat PTD–Es was also distributed in the retina after eye-drop administration, while Es did not appear in the retina in the eye-drop group, which indicates that Tat PTD–Es had stronger penetrating ability *in vivo*, and could penetrate the ocular barriers and arrive at the retina after eye-drops, while Es could not.

3.7. Inhibition effects of Tat PTD–Es on CNV generation

Mouse CNV models were established by laser burning. Tat PTD–Es or Es was eye-dropped or intravitreally injected. Eye-dropped NS was used as a negative control, and intravitreally injected Avastin was used as a positive control (Fig. 10). The CNV areas of mice intravitreally injected with Tat PTD–Es and Es were 961.2 ± 86.9 μm^2 and 944.6 ± 88.3 μm^2, respectively, which was less than the negative control (2623.6 ± 240.9 μm^2; $p < 0.01$), and was not significantly different from the positive control (863.5 ± 50.1 μm^2). When Es was administered *via* eye-drops, the CNV area was 2514.7 ± 260.7 μm^2, which was not significantly different from the negative control, showing no inhibitory effects on CNV. The CNV area of Tat PTD–Es eye-drop mice was 1378.4 ± 154.3 μm^2, which was significantly less than the negative control ($p < 0.01$). Therefore, the Tat PTD–Es eye-drops were capable of inhibiting CNV angiogenesis, and these results demonstrate that Tat PTD–Es had the capacity to penetrate the ocular barriers, reach the retina choroid and play its roles in the fundus oculi *via* eye-drops.

4. Discussion

In our study, though His-tag and Tat PTD were fused to the *N*-terminus of Es protein, no activity decrease was detected. Tat PTD–Es even displayed an enhanced inhibitory effect on EAHY926 cells compared with Es ($p < 0.05$) at low concentrations (0.2 and 0.8 μM), which implies that the fusion of Tat PTD to Es enhanced the inhibitory activity of Es on endothelial cells.

In the activity assay, both Tat PTD–Es and Es displayed excellent ability to inhibit endothelial cell proliferation. Tat PTD–Es even resulted in higher inhibition than Es at low concentrations. It might be caused by more translocation of Tat PTD–Es into cells. This point was substantiated by *in vitro* cellular uptake studies, in which Tat PTD could favour the delivery of Es into cells.

In terms of the internalization kinetics of Tat PTD–Es into EAHY926 cells, systematic studies were carried out. Direct translocation was not excluded as a potential pathway for Tat PTD–Es into EAHY926 cells, since the entrance of Tat PTD–Es into cells was not prevented completely at low temperature or in the presence of NaN_3, although it was obviously reduced, which indicates that a small portion of Tat PTD–Es could still penetrate the cell membrane without the energy *via* direct translocation. Some studies came to similar conclusions [30–32]. Hypertonic sucrose and chlorpromazine are known to block clathrin-mediated endocytosis. The results suggested that Tat PTD–Es entered EAHY926

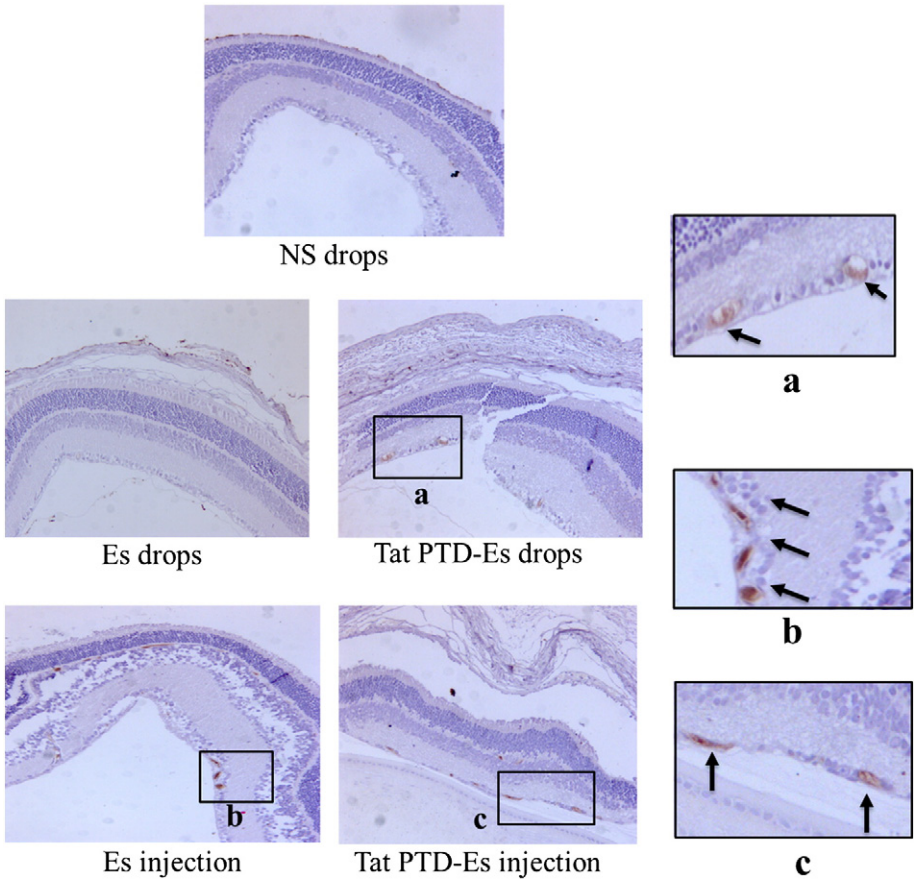

Fig. 9. Immunohistochemistry of mouse eyes.

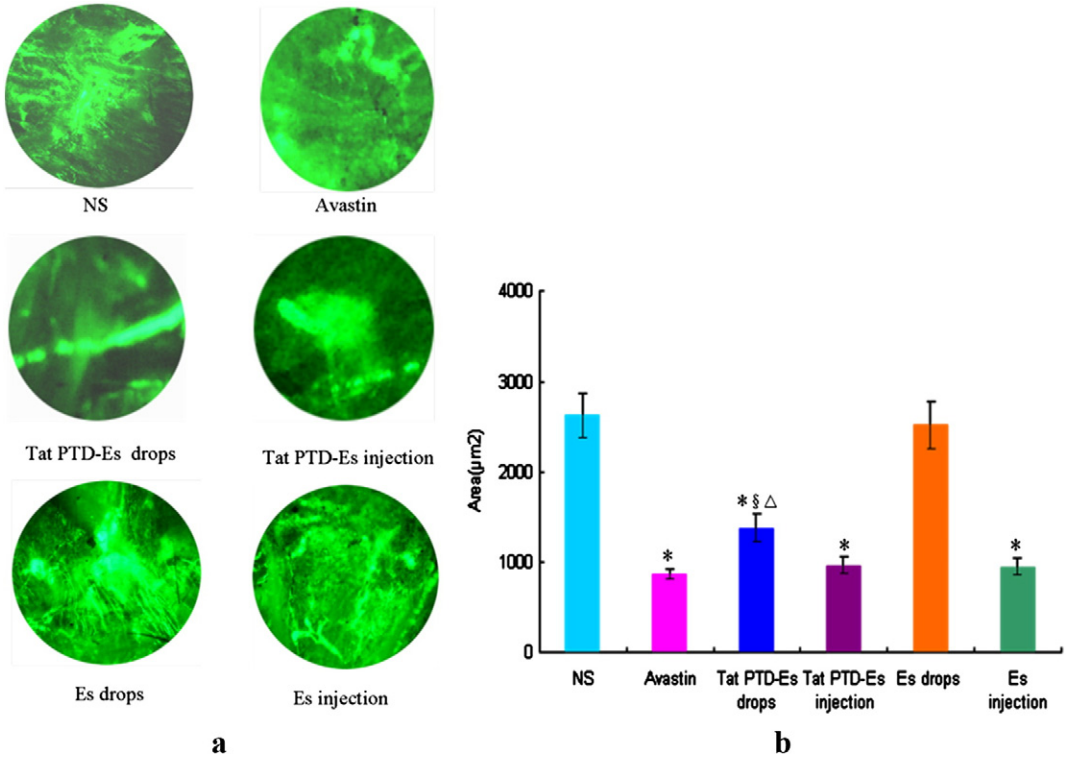

Fig. 10. The inhibition effects of Tat PTD–Es on CNV generation. a. The fluorescent images of CNV (×40). b. The CNV areas of different groups (area, $\bar{x} \pm s$, $n = 5$) $^{*}p < 0.01$ *vs.* NS group; $^{\S}p < 0.05$ *vs.* Avastin group; $^{\triangle}p < 0.05$ *vs.* Tat PTD–Es injection.

cells by clathrin-mediated endocytosis. In addition, the results showed that a relatively small portion of Tat PTD–Es got into the cells *via* caveolae-mediated endocytosis. Inhibitors of macropinocytosis greatly reduced the uptake of Tat PTD–Es into EAHY926 cells. In summary, Tat PTD–Es uptake by EAHY926 cells was mainly *via* endocytosis and several pathways involved in its internalization.

Macropinocytosis was a dominant route of Tat PTD–Es internalization into the cells. Tat PTD was reported to follow the macropinocytosis pathway in some studies [33–35]. Macropinocytosis was reported to be a major route of entry for positively charged molecules [36], because of the membrane-bound negatively charged proteoglycans, such as heparan sulphate. The negatively charged proteoglycans act as receptors for positively charged molecules and might be involved in stimulating endocytic uptake. Tat PTD–Es endow high positive charges, so we speculate that strong and multiple bonds between the positive protein and the negatively charged surface proteoglycans will cause a large number of proteins to accumulate on the cell membrane, and induce cytoskeleton rearrangement, resulting in the initiation of ruffle formation followed by uptake *via* macropinocytosis.

Though different mechanisms are involved in the entry of Tat PTD–Es into cells, there is no doubt about its ability to translocate into cells. Conjugating Tat PTD with Es not only retained the anti-angiogenesis activity of Es, but also boosted its permeability into cells, which might allow Tat PTD–Es to cross the ocular barrier and play its activity in fundus oculi.

It is known that many drugs are prevented from reaching the fundus oculi by ocular barriers and remain at the ocular surface after eye-drop administration. As the blood flow of eyes is abundant, even for drugs with the ability to penetrate corneal barriers, they will quickly be brought into the systemic circulation when passing through blood–eye barriers, and the amount of drugs in the fundus oculi is scarce. So, in order to accumulate a higher drug concentration, more administration times (6 times per day) and longer times (3 days) were used in the Tat PTD–Es eye-drop experiments. The results showed that Tat PTD–Es exhibited stronger penetration power than Es in crossing the ocular barrier, in which after eye-drop administration, Tat PTD–Es was detectable in the retina, while Es was not. The results suggest that Tat PTD could allow Es to cross corneal barriers, conjunctival barriers and blood–retina barriers, and transport Es to the fundus oculi from the ocular surface. Tat PTD–Es eye-drops may be applicable for curing fundus oculi vascular proliferation diseases.

For a full evaluation of Tat PTD–Es, mice CNV models were used to assess its inhibitory effects on choroidal neovascularization. Intravitreal injection is commonly used as an efficient route in clinical treatment, so we used this administration route to assess the anti-angiogenesis effects of Tat PTD–Es and Es *in vivo*. Both of them displayed an inhibitory action on CVN after intravitreal injection, which further indicates that Tat PTD–Es and Es has anti-angiogenesis activities *in vivo*. When administrated by eye-drops, Tat PTD–Es exhibited a suppressive function on CNV, while Es did not. Different penetration capability might give rise to the results. After being fused to Tat PTD, Es had high permeability to cross ocular barriers, arrived in fundus oculi, such as the retina and choroid, and further showed inhibitory effects on CNV. Additionally, when preparing choroidal auxiliary pieces, bleeding inside the eye was observed in intravitreally injected mice, while no such phenomenon was found in the eye-drop groups. Therefore, there was less impairment to eyes for eye-drop administration than for intravitreal injection. In clinical treatment, eye-drops are an ideal and more acceptable method for ocular administration. Our research made Es administration *via* eye-drops possible, which may provide a means to explore administration of proteins and other macromolecules in the treatment of fundus oculi diseases.

However, some elaborate studies should be conducted. For instance, the pathway of Tat PTD–Es across eye barriers and its distribution in different ocular tissues have not been determined, which needs to be further investigated. Furthermore, various models, such as diabetic retinopathy, should be established to acquire more ocular pharmacodynamic information of Tat PTD–Es.

Conflict of interest

We declare that we have no conflict of interest.

Acknowledgements

This work was supported by the National Natural Science Foundation of China under grant No. 81273417 and No. 81302686.

References

[1] M.S. O'Reilly, T. Boehm, Y. Shing, N. Fukai, G. Vasios, W.S. Lane, E. Flynn, J.R. Birkhead, B.R. Olsen, J. Folkman, Endostatin: an endogenous inhibitor of angiogenesis and tumor growth, Cell 88 (1997) 277–285.
[2] J. Folkman, Antiangiogenesis in cancer therapy—endostatin and its mechanisms of action, Exp. Cell Res. 312 (2006) 594–607.
[3] M. Dhanabal, R. Volk, R. Ramchandran, M. Simons, V.P. Sukhatme, Cloning, expression, and in vitro activity of human endostatin, Biochem. Biophys. Res. Commun. 258 (1999) 345–352.
[4] H.L. Xu, H.N. Tan, F.S. Wang, W. Tang, Research advances of endostatin and its short internal fragments, Curr. Protein Pept. Sci. 9 (2008) 275–283.
[5] H. Tan, S. Yang, Y. Feng, C. Liu, J. Cao, G. Mu, F. Wang, Characterization and secondary structure analysis of endostatin covalently modified by polyethylene glycol and low molecular weight heparin, J. Biochem. 144 (2008) 207–213.
[6] H. Tan, G. Mu, W. Zhu, J. Liu, F. Wang, Down-regulation of vascular endothelial growth factor and up-regulation of pigment epithelium derived factor make low molecular weight heparin–endostatin and polyethylene glycol–endostatin potential candidates for anti-angiogenesis drug, Biol. Pharm. Bull. 34 (2011) 545–550.
[7] A. Sturzu, S. Sheikh, H. Echner, T. Nagele, M. Deeg, C. Schwentner, M. Horger, U. Ernemann, S. Heckl, Novel bourgeonal fragrance conjugates for the detection of prostate cancer, Invest. New Drugs 31 (2013) 1151–1157.
[8] I. Okamoto, K. Aoe, T. Kato, Y. Hosomi, A. Yokoyama, F. Imamura, K. Kiura, T. Hirashima, M. Nishio, N. Nogami, H. Okamoto, H. Saka, N. Yamamoto, N. Yoshizuka, R. Sekiguchi, K. Kiyosawa, K. Nakagawa, T. Tamura, Pemetrexed and carboplatin followed by pemetrexed maintenance therapy in chemo-naive patients with advanced nonsquamous non-small-cell lung cancer, Invest. New Drugs 31 (2013) 1275–1282.
[9] I. Garrido-Laguna, K.A. McGregor, M. Wade, J. Weis, W. Gilcrease, L. Burr, R. Soldi, L. Jakubowski, C. Davidson, G. Morrell, J.D. Olpin, K. Boucher, D. Jones, S. Sharma, A phase I/II study of decitabine in combination with panitumumab in patients with wild-type (wt) KRAS metastatic colorectal cancer, Invest. New Drugs 31 (2013) 1257–1264.
[10] A.D. Frankel, C.O. Pabo, Cellular uptake of the tat protein from human immunodeficiency virus, Cell 55 (1988) 1189–1193.
[11] E. Vives, P. Brodin, B. Lebleu, A truncated HIV-1 Tat protein basic domain rapidly translocates through the plasma membrane and accumulates in the cell nucleus, J. Biol. Chem. 272 (1997) 16010–16017.
[12] S.R. Schwarze, A. Ho, A. Vocero-Akbani, S.F. Dowdy, In vivo protein transduction: delivery of a biologically active protein into the mouse, Science 285 (1999) 1569–1572.
[13] E. Gullotti, J. Park, Y. Yeo, Polydopamine-based surface modification for the development of peritumorally activatable nanoparticles, Pharm. Res. 30 (2013) 1956–1967.
[14] H. Brooks, B. Lebleu, E. Vives, Tat peptide-mediated cellular delivery: back to basics, Adv. Drug Deliv. Rev. 57 (2005) 559–577.
[15] M. Rapoport, H. Lorberboum-Galski, TAT-based drug delivery system—new directions in protein delivery for new hopes? Expert Opin. Drug Deliv. 6 (2009) 453–463.
[16] E. Vives, Present and future of cell-penetrating peptide mediated delivery systems: "is the Trojan horse too wild to go only to Troy?", J. Control. Release 109 (2005) 77–85.
[17] Y. Wang, H. Lin, S. Lin, J. Qu, J. Xiao, Y. Huang, Y. Xiao, X. Fu, Y. Yang, X. Li, Cell-penetrating peptide TAT-mediated delivery of acidic FGF to retina and protection against ischemia–reperfusion injury in rats, J. Cell. Mol. Med. 14 (2010) 1998–2005.
[18] X. Zhang, F. Wang, Intracellular transduction and potential of Tat PTD and its analogs: from basic drug delivery mechanism to application, Expert Opin. Drug Deliv. 9 (2012) 457–472.
[19] S. Batool, M.S. Nawaz, M.A. Kamal, In silico analysis of the amido phosphoribosyltransferase inhibition by PY873, PY899 and a derivative of isophthalic acid, Invest. New Drugs 31 (2013) 1355–1363.
[20] X. Pan, Y. Wang, M. Zhang, W. Pan, Z.T. Qi, G.W. Cao, Effects of endostatin–vascular endothelial growth inhibitor chimeric recombinant adenoviruses on anti-angiogenesis, World J. Gastroenterol. 10 (2004) 1409–1414.
[21] F. Girolamo, G. Elia, M. Errede, D. Virgintino, S. Cantatore, L. Lorusso, L. Roncali, M. Bertossi, L. Ambrosi, In vivo assessment of epichlorohydrin effects: the chorioallantoic membrane model, Med. Sci. Monit. 12 (2006) BR21–BR27.
[22] N. Ishimoto, T. Nemoto, K. Nagayoshi, F. Yamashita, M. Hashida, Improved antioxidant activity of superoxide dismutase by direct chemical modification, J. Control. Release 111 (2006) 204–211.
[23] T. Tobe, S. Ortega, J.D. Luna, H. Ozaki, N. Okamoto, N.L. Derevjanik, S.A. Vinores, C. Basilico, P.A. Campochiaro, Targeted disruption of the FGF2 gene does not prevent

choroidal neovascularization in a murine model, Am. J. Pathol. 153 (1998) 1641–1646.
[24] C. Liu, W. Yu, Z. Chen, J. Zhang, N. Zhang, Enhanced gene transfection efficiency in CD13-positive vascular endothelial cells with targeted poly(lactic acid)–poly(ethylene glycol) nanoparticles through caveolae-mediated endocytosis, J. Control. Release 151 (2011) 162–175.
[25] T. Letoha, S. Gaal, C. Somlai, Z. Venkei, H. Glavinas, E. Kusz, E. Duda, A. Czajlik, F. Petak, B. Penke, Investigation of penetratin peptides. Part 2. In vitro uptake of penetratin and two of its derivatives, J. Pept. Sci. 11 (2005) 805–811.
[26] X. Zhang, Y. Jin, M.R. Plummer, S. Pooyan, S. Gunaseelan, P.J. Sinko, Endocytosis and membrane potential are required for HeLa cell uptake of R.I.-CKTat9, a retro-inverso Tat cell penetrating peptide, Mol. Pharm. 6 (2009) 836–848.
[27] U.S. Huth, R. Schubert, R. Peschka-Suss, Investigating the uptake and intracellular fate of pH-sensitive liposomes by flow cytometry and spectral bio-imaging, J. Control. Release 110 (2006) 490–504.
[28] S.K. Lai, K. Hida, S.T. Man, C. Chen, C. Machamer, T.A. Schroer, J. Hanes, Privileged delivery of polymer nanoparticles to the perinuclear region of live cells via a non-clathrin, non-degradative pathway, Biomaterials 28 (2007) 2876–2884.
[29] H. Raghu, N. Sharma-Walia, M.V. Veettil, S. Sadagopan, B. Chandran, Kaposi's sarcoma-associated herpesvirus utilizes an actin polymerization-dependent macropinocytic pathway to enter human dermal microvascular endothelial and human umbilical vein endothelial cells, J. Virol. 83 (2009) 4895–4911.
[30] G. Ter-Avetisyan, G. Tunnemann, D. Nowak, M. Nitschke, A. Herrmann, M. Drab, M.C. Cardoso, Cell entry of arginine-rich peptides is independent of endocytosis, J. Biol. Chem. 284 (2009) 3370–3378.
[31] E. Eiriksdottir, I. Mager, T. Lehto, S. El Andaloussi, U. Langel, Cellular internalization kinetics of (luciferin-)cell-penetrating peptide conjugates, Bioconjug. Chem. 21 (2010) 1662–1672.
[32] S. Futaki, I. Nakase, A. Tadokoro, T. Takeuchi, A.T. Jones, Arginine-rich peptides and their internalization mechanisms, Biochem. Soc. Trans. 35 (2007) 784–787.
[33] T. Letoha, A. Keller-Pinter, E. Kusz, C. Kolozsi, Z. Bozso, G. Toth, C. Vizler, Z. Olah, L. Szilak, Cell-penetrating peptide exploited syndecans, Biochim. Biophys. Acta 1798 (2010) 2258–2265.
[34] A.T. Jones, Macropinocytosis: searching for an endocytic identity and role in the uptake of cell penetrating peptides, J. Cell. Mol. Med. 11 (2007) 670–684.
[35] I. Nakase, M. Niwa, T. Takeuchi, K. Sonomura, N. Kawabata, Y. Koike, M. Takehashi, S. Tanaka, K. Ueda, J.C. Simpson, A.T. Jones, Y. Sugiura, S. Futaki, Cellular uptake of arginine-rich peptides: roles for macropinocytosis and actin rearrangement, Mol. Ther. 10 (2004) 1011–1022.
[36] I.A. Khalil, K. Kogure, S. Futaki, H. Harashima, High density of octaarginine stimulates macropinocytosis leading to efficient intracellular trafficking for gene expression, J. Biol. Chem. 281 (2006) 3544–3551.